Effect of Process Conditions on Birefringence Development in Injection-Molded Parts. I. Numerical Analysis

SHIA CHUNG CHEN* and YUNG CHENG CHEN

Mechanical Engineering Department, Chung Yuan University, Chung Li, Taiwan 32023, Republic of China

SYNOPSIS

Analysis of the injection-molding process based on Leonov viscoelastic fluid model has been employed to study the effects of process conditions on the residual stress and birefringence development in injection-molded parts during the entire molding process. An integrated formulation was derived and numerically implemented to solve the nonisothermal, compressible, and viscoelastic nature of polymer melt flow. Simulations under process conditions of different melt temperatures, mold temperatures, filling speeds, and packing pressures are performed to predict the birefringence variation in both gapwise and planar direction. It has been found that melt temperature and the associated frozen layer thickness are the dominant factors that determine the birefringence development within the molded part. For a higher mold temperature, melt temperature, and injection speed, the averaged birefringence along gapwise direction is lower. The birefringence also increases significantly with the increased packing pressure especially along gate area. The simulated results show good consistency with those measured experimentally. © 1995 John Wiley & Sons, Inc.

INTRODUCTION

Injection molding is one of the most important polymer processing operations. The injection molding process consists of three major stages including filling, packing, and cooling. In the filling stage, hot molten polymer is injected into the mold cavity. Once the cavity is filled, additional polymer melt is forced into the cavity under high pressure in order to compensate for the subsequent shrinkage due to the solidification.

In recent years, simulations of the injection molding process based on inelastic fluid models have attracted attention and have been applied in the computer-aided engineering (CAE) area of plastics.[1-10] It is generally accepted that the Hele–Shaw type of flow model provides a reasonably accurate description of flow behavior in the thin-wall cavities. These simulations provide valuable information about process operations such as injection speed, injection pressure, melt front advancements, melt temperature distribution, holding pressure and holding time, etc. From these numerical predictions, the mold designer can improve the mold design and the molding performance. On the other hand, request for high-quality, defect-free parts has been increasing because of the extensive application of plastics in all areas of industry. Formation of part defects, such as uneven shrinkage, warpage, sink marks, residual stress, and birefringence may result from the entire history of all injection molding stages. These processing-induced defects remain tough issues to be solved from one mold design to the next. Although current CAE has as a goal the prediction of part quality, it is still in the initial development stage. For example, warpage analysis has been developed and performed in a qualitative way, its contribution from the flow residual stress is not known due to the inelastic nature of the viscous fluid model used in these analyses. In addition, quality and performance of many injection-molded optical parts are critical to the flow-induced residual stress, molecular orientation and the corresponding birefringence. It is, therefore, essential to understand the viscoelastic nature of polymer flow and the flow-induced residual stress development during the entire molding process. Once the simulations based on

* To whom correspondence should be addressed.

Journal of Applied Polymer Science, Vol. 55, 1757–1769 (1995)
 CCC 0021-8995/95/131757-13

the viscoelastic model have been developed, effects of processing parameters on the formation of residual stress and/or birefringence can be understood in more detail.

Numerical simulation of a viscoelastic flow is a difficult task. Recent reviews have been reported.[11-15] The major difficulty arises because of the viscoelastic nature of a polymer fluid subjected to large elastic deformation during the molding process. Obviously, the mathematical formulation of the constitutive model plays a critical role in determining the success of the numerical simulation of a viscoelastic fluid flow. Among different viscoelastic models employed for the simulation of injection molding, the Leonov model seems to be more flexible and has promising capability in describing the viscoelastic nature of polymer melt.[16-23] In previous studies,[16,20-22] attention has concentrated on the analysis of the filling process. The viscoelastic behavior of the polymer melt during the packing process has not been incorporated into these analyses. It has been found recently from birefringence measurements[24,25] that the packing pressure plays an important role in the determination of part residual stress. Therefore, the integrated simulation for the entire injection molding process is required essentially. Also, numerical treatment using equivalent viscosity associated with shear rate[20,22] as the convergence criterion during iterations may not only result in instability for a small shear rate value but also require expensive computations. Lately, simulations of filling and the postfilling stages based on the Leonov viscoelastic model have been developed in an integrated formulation.[26] The pressure field can be formulated into a nonlinear form of a Poisson-type equation and found to be easier and more stable for numerical implementation. Through these simulations, effects of processing parameters on the part properties resulting from the viscoelastic nature of polymer melt during the whole injection molding process can be predicted and investigated. In this work, effects of processing parameters including melt temperature, mold temperature, injection speed, and packing pressure on the birefringence development in the injection-molded part are simulated and discussed. Analysis results are also verified by birefringence measurement of which the detailed experimental works were reported in separate paper.[25]

THEORETICAL FORMULATION

The mathematical modeling and the assumptions used for the simulation of the injection molding process are basically similar to those of previous studies.[4-10] The relevant components of the governing equations for continuity, momentum, and energy describing the injection molding of a simple plate in terms of the Hele-Shaw flow model are

$$\frac{\partial P}{\partial t} + \frac{\partial}{\partial x}(\rho U) = 0 \tag{1}$$

$$\frac{\partial P}{\partial x} = \frac{\partial}{\partial z}(\tau_{xz}) \tag{2}$$

$$\rho C_p\left(\frac{\partial T}{\partial t} + U\frac{\partial T}{\partial x}\right) = \frac{\partial}{\partial z}\left(K\frac{\partial T}{\partial z}\right) + \phi \tag{3}$$

where t is the time, ρ the density, C_p the specific heat, K the thermal conductivity, P the pressure, T the temperature, z the gapwise direction, τ_{xz} the shear stress in the x direction, and U the gapwise injection velocity in the x direction. The term ϕ is the dissipation function defined elsewhere.[26,27] The corresponding boundary conditions for the filling process are

$$P|_{\text{melt front}} = 0 \tag{4a}$$

$$\bar{U}|_{\text{inlet}} = \frac{1}{b}\int_0^b U\,dz = \frac{Q}{2bW} \tag{4b}$$

$$T(t)|_{\text{inlet}} = T_{\text{melt}} \tag{4c}$$

$$U(b) = U(-b) = 0 \tag{4d}$$

$$T(b) = T(-b) = Tw \tag{4e}$$

where Q represents the injection flow rate, $\bar{U}$ the averaged velocity in the gapwise direction, T_{melt} the inlet melt temperature, T_W the mold cavity wall temperature, W the width of the plate, and b the half-cavity thickness. In the packing and cooling stages, boundary conditions for the filling stage in Eqs. (4a) and (4b) are replaced by

$$P|_{\text{inlet}} = P_{\text{packing}}(t) \tag{4f}$$

The constitutive equations used for the analysis comprise the Leonov viscoelastic model[17-19] described by

$$\frac{\partial C_k}{\partial t} + V\nabla C_k - (\nabla V)^T|C_k - C_k|\nabla V + \frac{1}{2\theta_k}(C_k|C_k - I) = 0 \tag{5}$$

$$\tau = -PI + s\eta_0(\nabla V + \nabla V^T) + \sum_{k=1}^{N} \frac{\eta_k}{\theta_k} C_k \quad (6)$$

$$\eta_0 = \sum_{k=1}^{N} \frac{\eta_k}{1-s} \quad (7)$$

where η_0 is the zero-shear-rate viscosity, η_k the shear viscosity of the kth mode, θ_k the relaxation time of the kth node and s a rheological constant ($0 < s < 1$); N is the number of the modes in the Leonov model, V the velocity vector, I the unit tensor, τ the stress tensor, and C_k the elastic strain tensor of the kth mode. For self-consistency there is a constraint on C_k such that

$$\det[C_k] = 1 \quad (8)$$

The temperature dependence of η_0, η_k, and θ_k is based on the Williams–Laudel–Ferry (WLF) shift factor a_T, namely $\theta_k(T) = \theta_k(T_0)a_T/a_{T_0}$ and $\eta_k(T) = \eta_k(T_0)a_T/a_{T_0}$ where

$$a_T = \begin{cases} a_{T_g} & T \le T_g \\ \exp\left[-\dfrac{C_1(T - T_{\text{ref}})}{C_2 + T - T_{\text{ref}}}\right] & T > T_g \end{cases} \quad (9)$$

T_{ref} is the reference temperature, T_g the glass transition temperature, and C_1 and C_2 are constants.

For a three-dimensional thin part, the polymer melt flow in the cavity is basically two-dimensional from the local coordinate point of view. Also, due to the uniform melt front velocity in the width direction for an injection plate with a line gate at the entrance, the components of C_k in Eq. (5) can be reduced to

$$\frac{\partial C_{xx,k}}{\partial t} + U\frac{\partial C_{xx,k}}{\partial x} - 2\frac{\partial U}{\partial z} C_{xz,k} + \frac{1}{2\theta_k}(C_{xx,k}^2 + C_{xz,k}^2 - 1) \quad (10a)$$

$$\frac{\partial C_{xz,k}}{\partial t} + U\frac{\partial C_{xz,k}}{\partial x} - \frac{\partial U}{\partial z} C_{zz,k} + \frac{1}{2\theta_k}(C_{xx,k}C_{xz,k} + C_{xz,k}C_{zz,k}) = 0 \quad (10b)$$

$$\frac{\partial C_{zz,k}}{\partial t} + U\frac{\partial C_{zz,k}}{\partial x} + \frac{1}{2\theta_k}(C_{xz,k}^2 + C_{zz,k}^2 - 1) = 0 \quad (10c)$$

under the constraint of

$$C_{xx,k}C_{zz,k} - C_{xz,k}^2 = 1 \quad (10d)$$

The initial values of Eq. (10) are evaluated from the fully developed, steady-state solutions given by

$$C_{xx,k}^{(0)} = \frac{\sqrt{2}\,Y}{\sqrt{1+Y}} \quad (11a)$$

$$C_{xz,k}^{(0)} = \frac{\Gamma}{1+Y} \quad (11b)$$

$$C_{zz,k}^{(0)} = \frac{\sqrt{2}}{\sqrt{1+Y}} \quad (11c)$$

$$\Gamma = 2\theta_k \frac{\partial U}{\partial z} \quad (11d)$$

$$Y(z) = \sqrt{1 + 4\theta_k^2\left(\frac{\partial U}{\partial z}\right)^2} \quad (11e)$$

under isothermal conditions. Numerical solutions of $C_{ij,k}$ values in Eq. (10) can be found elsewhere.[20,21,27,28]

Since the polymer melt is considered to be compressible, the change of melt density should follow a pressure–volume–temperature (PVT) relation. In this study, the Spencer–Gilmore type PVT equation is used and is given by

$$(P + \hat{P})\left(\frac{1}{\rho} - \frac{1}{\hat{\rho}}\right) = \hat{R}T \quad (12)$$

where $\hat{P}$, $\hat{\rho}$, and $\hat{R}$ are constants. Incorporating the PVT relation into Eqs. (1) and (2), an integrated formulation of Poisson-type equation can be obtained:

$$M(x, t, b, \rho, P)\frac{\partial P}{\partial t} - \left[\frac{\partial}{\partial x}\left(\frac{S_1}{b}\frac{\partial P}{\partial x}\right)\right] + \frac{1}{b}\left[\frac{\partial S_2}{\partial x}\right] = Q(x, t, b, T, P) \quad (13)$$

with

$$S_1 = \int_0^b \frac{z^2}{s\eta_0}\,dz \quad (14)$$

$$S_2 = \int_0^b \left(\frac{z}{s\eta_0}\sum_{k=1}^{N}\frac{\eta_k}{\theta_k} C_{xz,k}\right) dz \quad (15)$$

$$M = \frac{1}{b}\left(\frac{1}{P + \hat{P}}\right)\int_0^b \left(1 - \frac{\rho}{\hat{\rho}}\right) dz \quad (16)$$

$$Q = \frac{1}{b}\int_0^b \left(1 - \frac{\rho}{\hat{\rho}}\right)\frac{\partial \ln T}{\partial t}\,dz \quad (17)$$

Detailed derivations of Eqs. (13)–(17) can be found elsewhere.[26] S_1 can be considered as the fluidity or

the flow conductance, which is determined by the local cavity thickness and the Newtonian viscosity value of the polymer melt. S_2 represents the effects of the non-Newtonian behavior and the elastic nature of viscoelastic melt on the flow velocity. Equation (13) represents an integrated formulation in solving the pressure field for the entire injection molding process including filling, packing, and cooling phases. It has a similar form as that used in previous studies[4,5,10] based on the inelastic fluid model except that an additional term related to the gradient of S_2 is included. The present formulation not only has the advantage of avoiding the singularity problem and reducing numerical instability encountered in other studies,[20,22] but can also be easily extended from the previous numerical algorithms based on inelastic models.[4,5,10] The energy equation [Eq. (3)], the constitutive equations [Eq. (10)], and the PVT equation [Eq. (12)] are solved with the pressure equation [Eq. (13)] separately. Once the pressure, velocity, shear rate, elastic strain tensor, and stress tensor have been calculated, the first normal stress difference N_{1F}, the shear stress τ_{xz}, and the corresponding birefringence ΔN_F of flow-induced origin in the xz plane are computed according to the following equations:

$$N_{1F} = (\tau_{xx} - \tau_{zz})_F = 2 \sum_{k=1}^{N} \frac{\eta_k}{\theta_k} [C_{xx,k} - C_{zz,k}] \quad (18)$$

$$\tau_{xz} = 2 \sum_{k=1}^{N} \frac{\eta_k}{\theta_k} C_{xz,k} \quad (19)$$

$$\Delta N_F = C \, \Delta\tau = C[N_{1F}^2 + 4\tau_{xz}^2]^{1/2} \quad (20)$$

where C is the stress-optical coefficient taken as a value of $4.8 \times 10^{-9} m^3/N$.[16] The thermal-induced stresses are formulated under a plain strain condition, i.e., assuming that $\varepsilon_y = 0$, $\varepsilon_{zy} = 0$, and $\varepsilon_{xy} = 0$. As a result, the stress–strain relation can be described by

$$\tau_{xx} = \frac{E}{1 - \nu - 2\nu^2} [(1 - \nu)\varepsilon_x + \nu\varepsilon_z - \varepsilon_T] \quad (21)$$

$$\tau_{zz} = \frac{E}{1 - \nu - 2\nu^2} [\nu\varepsilon_x + (1 - \nu)\varepsilon_z - \varepsilon_T] \quad (22)$$

$$\tau_{xz} = \frac{E}{2(1 + \nu)} \varepsilon_{xz} \quad (23)$$

$$\tau_{yy} = \frac{E}{1 - \nu - 2\nu^2} [\varepsilon_x + \varepsilon_z - 2\varepsilon_T] \quad (24)$$

where ν is the Poisson's ratio, E is the Young's modulus, and α is the thermal expansion coefficient, and ΔT is the temperature difference. Stress τ_{yy} also exists. However, it does not contribute to the birefringence formation of thermal origin in the xz plane. Stresses in Eqs. (21)–(24) are solved using the principle of virtual work.[27] The first normal stress difference N_{1T} and the corresponding birefringence ΔN_T resulting from thermal stresses are therefore expressed by

$$N_{1T} = (\tau_{xx} - \tau_{zz})_T \quad (25)$$

$$\Delta N_T = C \, \Delta\tau = C[N_{1T}^2 + 4\tau_{xz}^2]^{1/2} \quad (26)$$

In the present cases, the order of ΔN_T is about one to two lower than that of ΔN_F under even cooling condition for both sides of mold cavity walls. There-

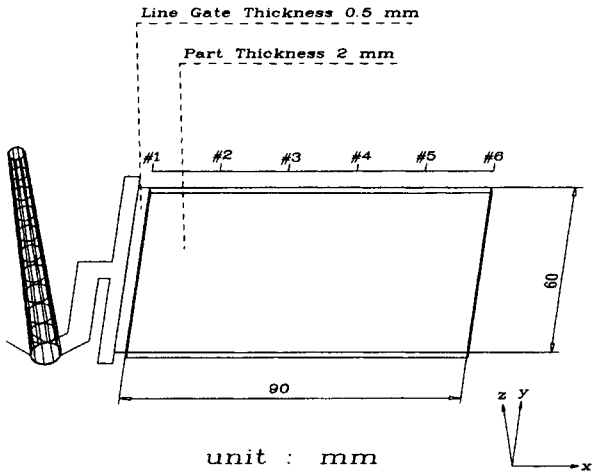

Figure 1 Geometry of the injection-molded plate.

Table I Material Properties of Polystyrene

1. Thermal Properties

   ρ = 940 kg/m^3, C_p = 2100 J/kg K) and K_p = 0.15 W/(m K)

2. Rheological Properties (Leonov viscoelastic model) at 463 K

   N = 2, s = 0.09, θ_1 = 0.8 s, θ_2 = 0.027 s, η_0 = 7000 Pa s, η_1 = 5440 Pa s, η_2 = 1500 Pa s, T_g = 373 K, T_{ref} = 407 K, C_1 = 20.378 K, C_2 = 101.6 K

3. Constants in Spencer–Gilmore type PVT Equation of State

   $\hat{P}$ = 186 MPa, $\hat{\rho}$ = 1220 kg/m^3, $\hat{R}$ = 80 J/(kg K)

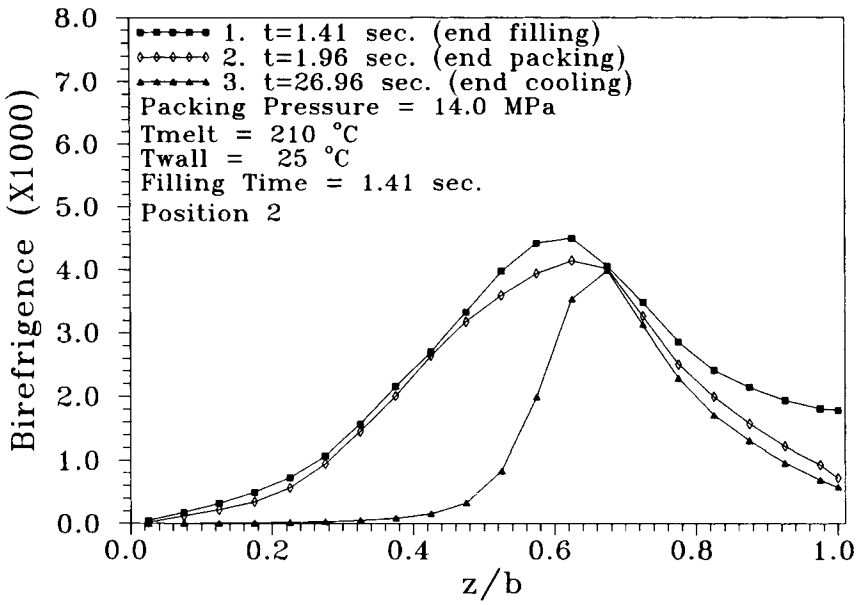

Figure 2 (a) Gapwise distribution of the birefringence Δn at the end of filling, packing, and cooling stages of the injection molding at location 2 under medium injection speed.

fore, the measured birefringence is assumed to be of flow-induced origin. In order to compare the simulated results with measured birefringence, gapwise averaged values of ΔN_F along flow direction are computed.

ANALYSIS PROCEDURE

Filling Stage Analysis

In the filling stage, the melt front advances at uniform velocity $\bar{U}$. The analysis interval Δt is taken

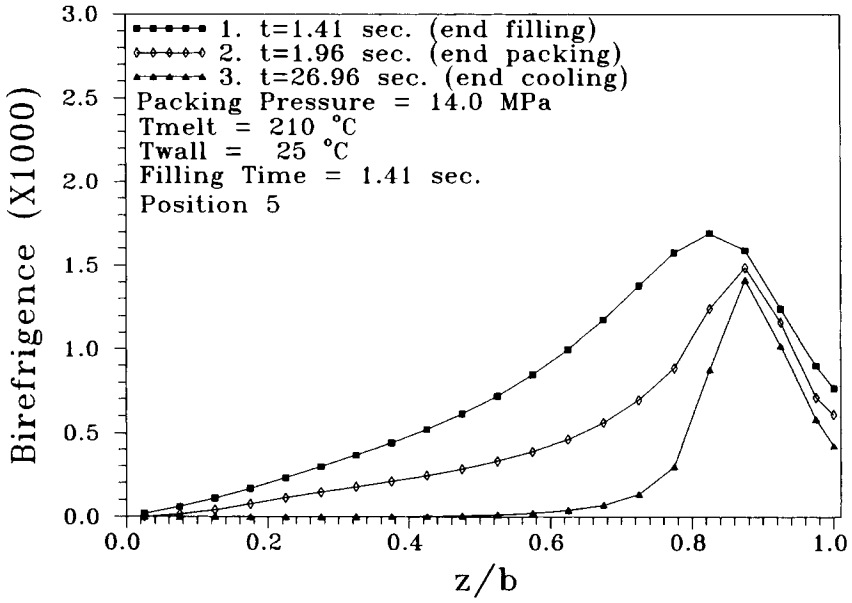

Figure 2 (b) Gapwise distribution of the birefringence Δn at the end of filling, packing, and cooling stages of the injection molding at location 5 under medium injection speed.

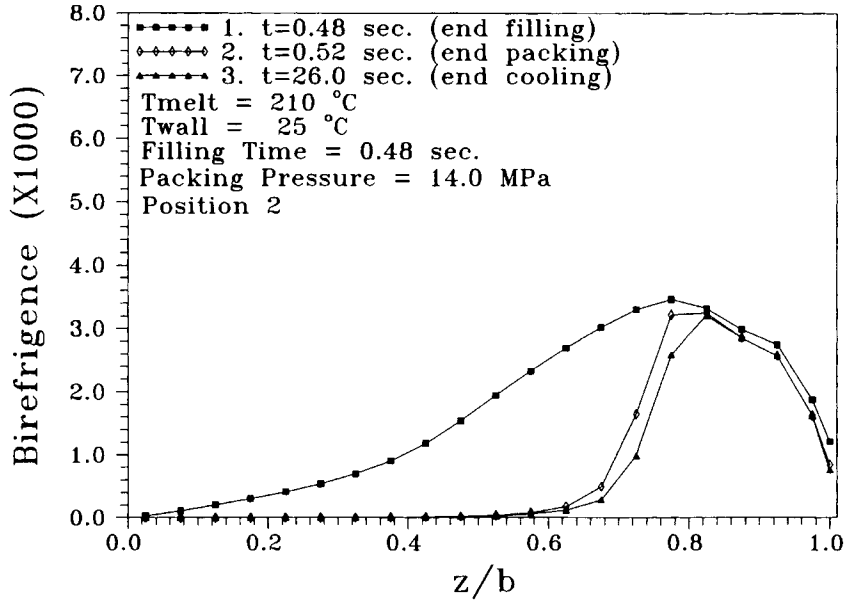

Figure 3 Gapwise distribution of the birefringence Δn at the end of filling, packing, and cooling stages of the injection molding at location 2 under high injection speed.

as 10^{-4} s. The distance between two finite-difference grid nodes is $L/\Delta t$, where L is the plate length. At the injection entrance, the melt temperature is assumed to be uniform. When polymer melt first enters the mold cavity, a Newtonian velocity profile is assumed. Then the associated shear rate values are used to calculate the initial values of $C_{ij,k}$. In the next time step, the energy equation is solved for gapwised temperature profile at each grid node from which new $C_{ij,k}$ values and τ_{xy} are calculated. Next, Eq. (13) is solved to obtain the pressure distribution and the pressure gradient from which shear rate and gapwise velocity profile can be further calculated using Eq. (2) and τ_{xy} value. With the new shear rate

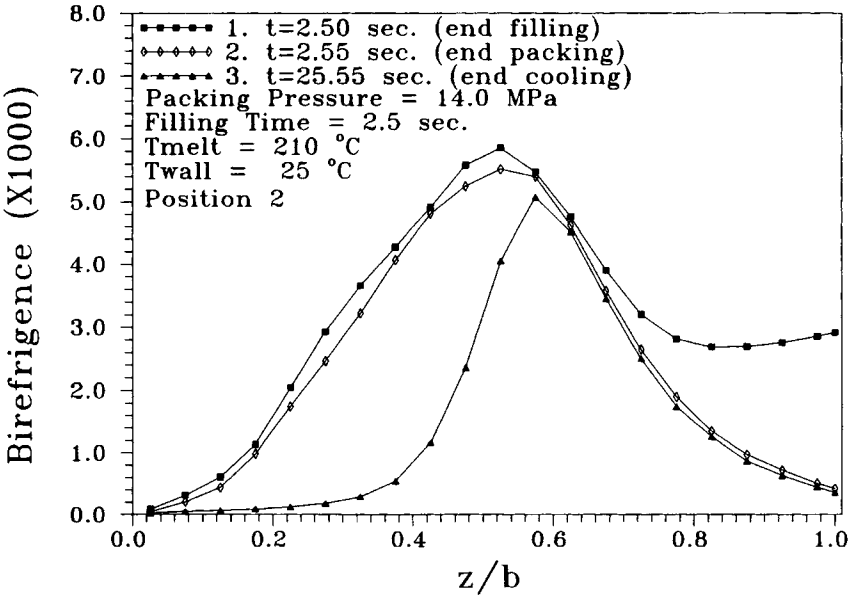

Figure 4 Gapwise distribution of the birefringence Δn at the end of filling, packing, and cooling stages of the injection molding at location 2 under low injection speed.

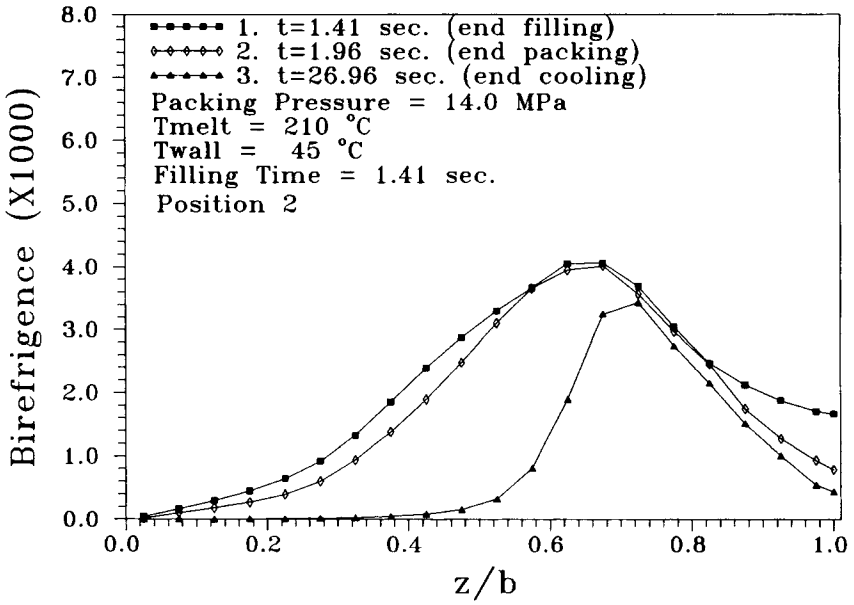

Figure 5 Gapwise distribution of the birefringence Δn at the end of filling, packing, and cooling stages of the injection molding at location 2 under high mold temperature.

values, iterations are conducted to recompute $C_{ij,k}$, τ_{xy}, pressure, pressure gradient, and the associated shear rate and velocity profile. Convergence criterion is set on shear rate values with a tolerance of 1%. Upon convergence, the simulation proceeds for the next time step until the plate cavity is completely filled.

Packing Stage Analysis

Values of $C_{ij,k}$, τ_{xy}, pressure, and temperature at the end of the filling process are used as the initial conditions for the packing stage. Equation (13) is first solved to obtain pressure and pressure gradient values at each grid node. Then shear rate and velocity

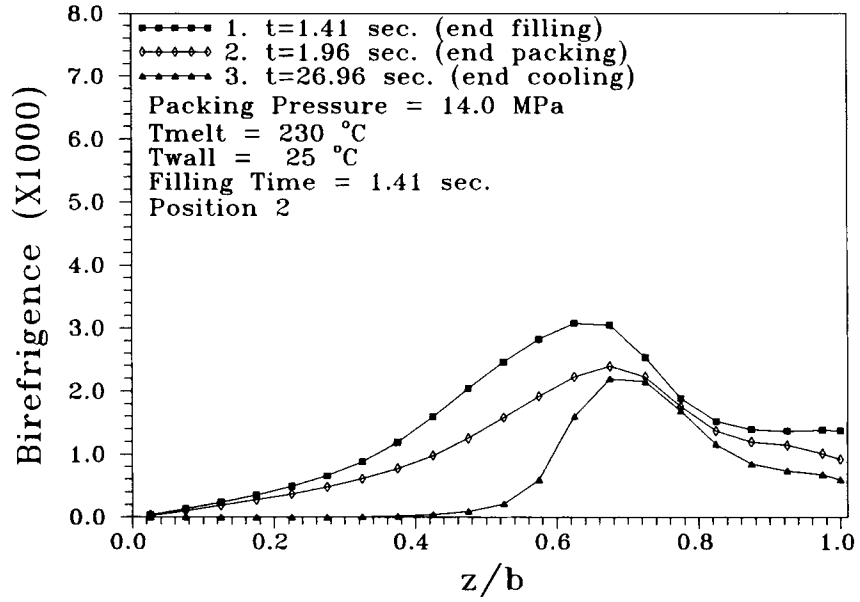

Figure 6 Gapwise distribution of the birefringence Δn at the end of filling, packing, and cooling stages of the injection molding at location 2 under high melt temperature.

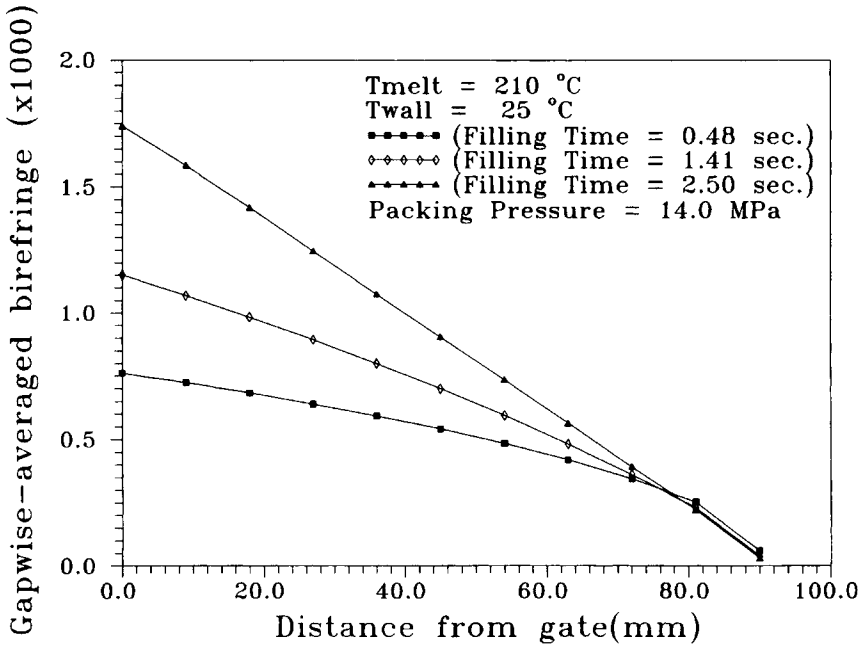

Figure 7 Distribution of the gapwise-averaged birefringence Δn along flow direction under various injection speed.

are calculated from Eq. (2). Values of $C_{ij,k}$ are then evaluated from which Eq. (13) is resolved in an iteration cycle till values of shear rate meet the convergence limit. During iterations, Eq. (12) is also used to compute a new density value, ρ. Once convergence is fulfilled, the energy equation is solved for the new temperature which is required for calculating new $C_{ij,k}$ values to be used in the next simulation step. The analysis proceeds until the temperature at the line gate reaches frozen temperature. The packing phase is assumed to be completed at this moment.

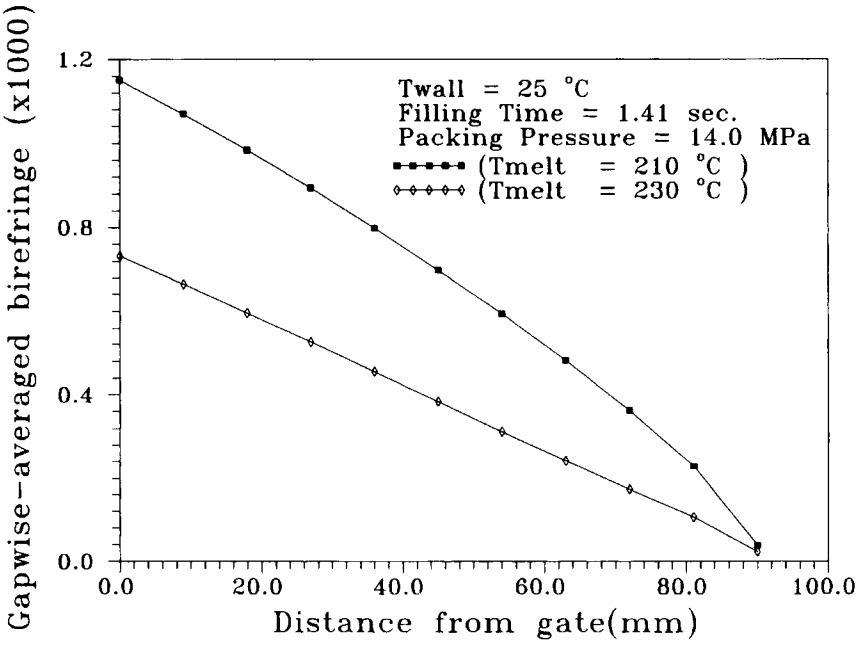

Figure 8 Distribution of the gapwise-averaged birefringence Δn along flow direction under various melt temperature.

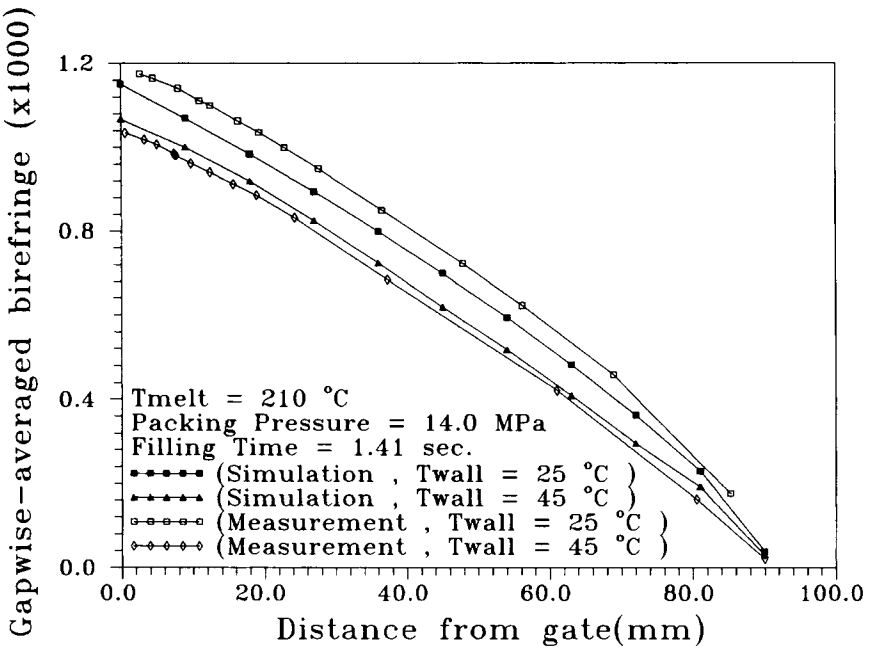

Figure 9 Distribution of the gapwise-averaged birefringence Δn along flow direction under various mold temperature.

Cooling Stage Analysis

In this solidification stage, the polymer melt is assumed to not flow. The energy equation is solved with the convection and dissipation terms neglected. In each time step, new $C_{ij,k}$ are recalculated to obtain the new stress and birefringence values. The pressure is also computed by Eq. (13). The simulation stops when the mold is opened.

A finite-difference method employed by control

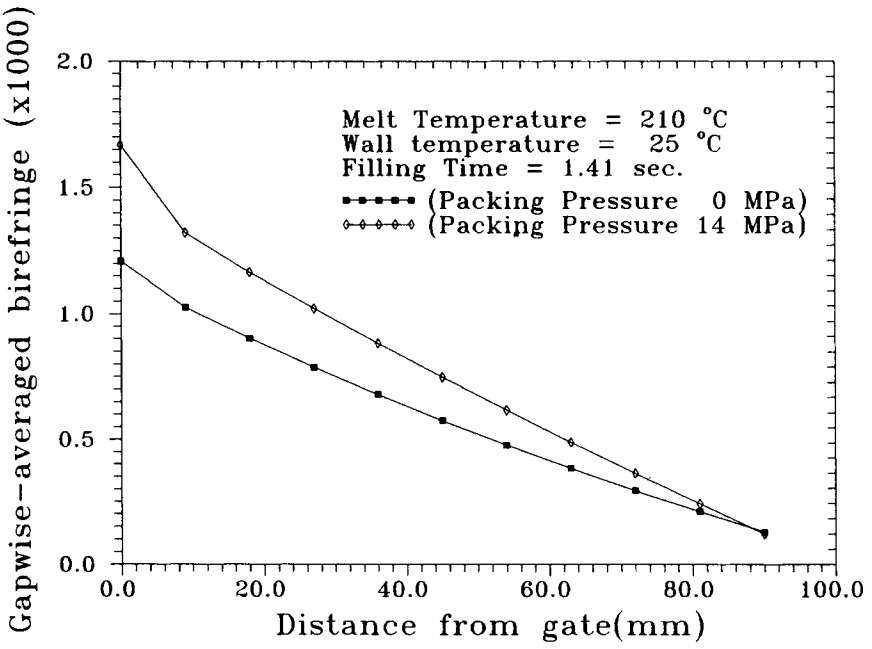

Figure 10 Distribution of the gapwise-averaged birefringence Δn along flow direction under various packing pressure.

volume formulation is applied to obtain the discretization equation for the nodal pressure [Eq. (12)]. The Crank–Nicolson numerical scheme was used for the energy equation. Explicit finite-difference scheme was used to solve the Leonov constitutive equations. Details can be found elsewhere.[26–28]

Birefringence Analysis

During every analysis step in all molding stages, ΔN_T and ΔN_F are calculated from Eqs. (20) and (26), correspondingly, once the shear stresses and first normal stress difference are obtained from the simulation. In addition to the gapwise profile of the birefringence, gap-averaged values of birefringence are also computed in order to compare with measured results.

ANALYSIS RESULTS AND DISCUSSIONS

In the present analysis, polystyrene (Styron 678U/Dow) was used. All material properties required for the analysis are listed in Table I. These data can be found in the literature.[16] Figure 1 illustrates the geometry schematic of a simple plate part 9 cm long, 6 cm wide, and 2 mm thick with a line-gate design. Different locations marked as numbers 1 to 6 are also indicated. The processing conditions, including injection temperature, mold temperature, filling time and packing pressure, are varied.

Figure 2(a) is the birefringence development during the filling, packing, and cooling stages of molding process at position 2. In the filling process, hot melt enters the mold cavity. Once the melt contacts the cold cavity wall, the melt starts to cool down near the cavity wall. The solidified thickness increases as the contact time with mold wall increases. Due to the fountain flow effect at the melt front and the small flow length of the present experimental part, the averaged melt temperature in the gapwise direction varies only slightly along flow direction. Near the gate area (position 2), thickness of the solidified layer is larger than that away from gate area (position 5). Therefore, velocity profile at position 2 becomes more sharply distributed with an increase in the maximum value at the gap center. Thus, the associated shear stress and shear rate as well as birefringence values also increase correspondingly. This situation can be clearly observed as seen by comparing birefringence values in Figs. 2(a) and 2(b). During the packing process, melt flow velocity and the associated shear rate are significantly reduced. The birefringence values are expected to decrease. However, the situation is not so obvious in the present injection speed. When the polymer melt was filling with a higher speed as the case of Figure 3, the birefringence value decreased dramatically around gap center. For a slower injection speed as represented in Figure 4, the birefringence does not show significant change during the packing stage similar to the case in Figure 2(a). This indicates that the relaxation is not intensive for a medium and slower injection speeds, which result in lower melt temperatures at the end of the filling process. Near the cavity wall where melt temperature was below glass transition temperature, T_g, flow stresses become frozen-in and show very slight relaxation afterward. In the cooling process, relaxation occurred only in the location where the melt was still hot in the beginning of the cooling phase. Within the solidified layer, frozen-in shear stress and normal stresses almost did not relax and remained to the end of the latter injection molding stage. When mold

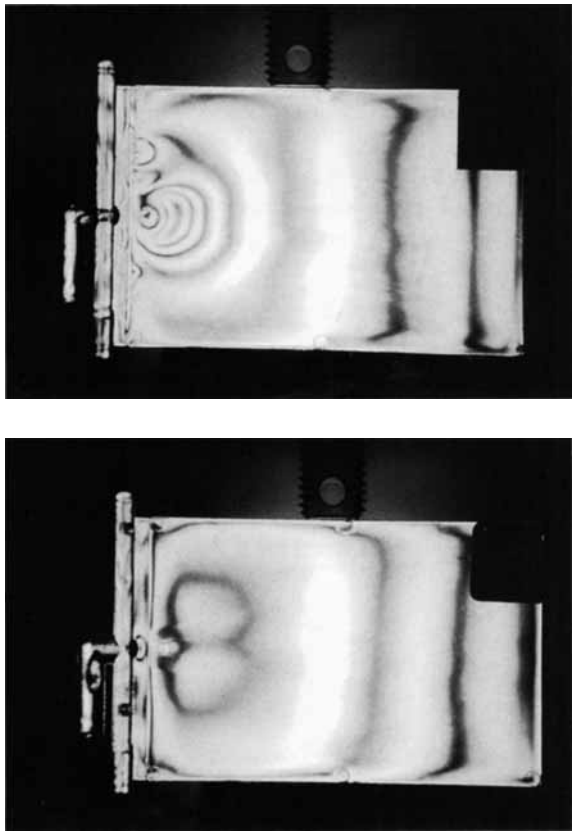

Figure 11 (a) Fringe pattern of the molded plate under 25°C mold temperature, 210°C melt temperature, 1.41-s filling time, and 14 MPa packing pressure (Ref. 25). (b) Fringe pattern of the molded plate under 45°C mold temperature, 210°C melt temperature, 1.41-s filling time, and 14 MPa packing pressure (Ref. 25).

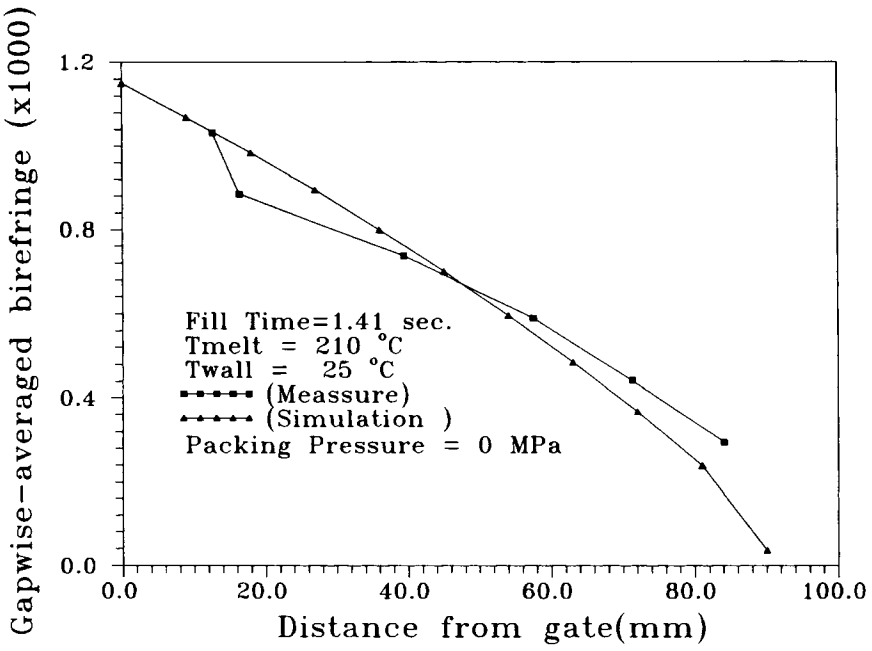

Figure 12 Distribution of the gapwise-averaged birefringence Δn along flow direction. Both experimental and simulated results are shown and compared.

temperature is increased from 25 to 45°C, the solidified thickness also decreases, and the velocity profile becomes less sharply distributed. The associated shear rate and birefringence decrease slightly with the maximum value occurring at a location closer to the cavity wall as seen in Figure 5. When melt temperature is increased from 210 to 230°C, relaxation occurs more rapidly. As a consequence, birefringence values at all stages are lower. In addition, more relaxation occurs during packing process. The

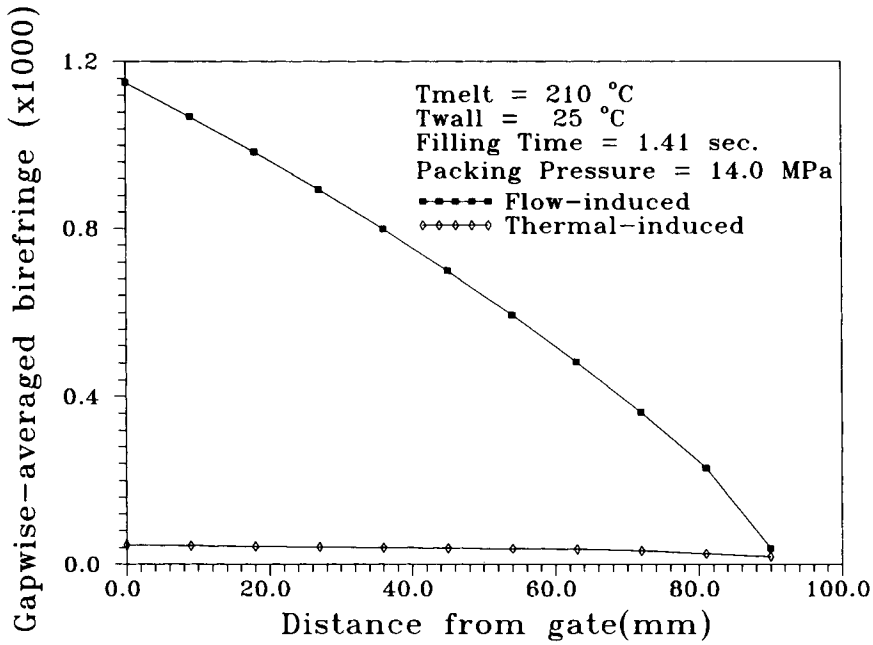

Figure 13 Simulated components of birefringence contributed from flow-induced residual stress and thermal-induced residual stress, respectively.

situations can be clearly seen in Figure 6. In summary, processing effects on gapwise-averaged birefringence distribution along flow direction are shown in Figures 7–10, respectively. Generally speaking, when the processing condition results in higher melt temperatures as well as thinner solidified layer, the associated residual stresses and birefringence are also lower. The simulated results were also compared with measured values. The detailed experimental works and comparisons are described in a separate study.[25] Here, only the fringe patterns related to change of mold temperature are illustrated as seen in Figures 11(a) and 11(b). The comparisons between analyzed results and experimental data under three different molding conditions were illustrated in Figures 9 and 12. Birefringence contributed from thermal stresses is small compared with those of flow-induced origin in present analyses as seen by one of the analyzed examples shown in Figure 13. Simulated results show good consistency with measured values in all case studies. The calculated birefringence distribution in gapwise direction also exhibits a maximum value near the cavity wall. This prediction is consistent with the observed results reported previously.[24]

CONCLUSIONS

1. Simulations of filling, packing, and cooling stages have been integrated to study the viscoelastic nature of polymer melt flow and the processing-induced birefringence development during injection molding. The integrated formulation leads to an efficient analysis numerically.
2. In the filling process, flow stresses arise due to the shear velocity gradient. When the melt front advances, gapwise temperature profile and solidified thickness also change. Gapwise velocity, the associated shear rate, and shear stress also vary with the maximum value shifting toward the gap center for a lower melt temperature and a thicker frozen layer. In the packing process, shear stresses decrease due to small flow velocities of polymer melt. The degree of relaxation depends on the temperature at melt core. Near the cavity wall, flow-induced stresses partially relaxed and become frozen within solidified layer. In the cooling stages, relaxation occurs in the hot melt. Frozen-in stresses almost remain to the end of cooling process.
3. It was found that melt temperature and the associated solidified thickness are the dominant factors that determine the birefringence development within the molded part. For a higher mold temperature, melt temperature, and injection speed, the averaged birefringence along the gapwise direction is lower.
4. The part birefringence also increases significantly with increased packing pressure especially around gate area.
5. The calculated birefringence are also compared with those measured experimentally. The analysis results show good consistency with measured values. This indicates that the present simulation is useful in the prediction of processing effect on part birefringence formation.

This work has been supported by a grant, NSC 81-0405-E033-04, from the National Science Council of Republic of China.

REFERENCES

1. M. R. Kamal and S. Kenig, *Polym. Eng. Sci.*, **12,** 295 (1972).
2. M. R. Kamal and S. Kenig, *Polym. Eng. Sci.*, **12,** 302 (1972).
3. C. A. Heiber and S. F. Shen, *J. Non-Newtonian Fluid Mech.*, **7,** 1 (1980).
4. V. W. Wang, C. A. Hieber, and K. K. Wang, *SPE Tech. Paper,* **32,** 97 (1986).
5. S. C. Chen, P. Pai, and C. Hsu, *SPE Tech. Paper,* **34,** 250 (1988).
6. Y. Kuo and M. R. Kamal, *Proceedings of International Conference on Polymer Processing,* MIT Press, Cambridge, MA, August 1977, p. 329.
7. T. S. Chung, *Polym. Eng. Sci.*, **25,** 772 (1985).
8. C. A. Hieber, G. Vandenengei, and H. H. Chiang, *SPE Tech. Paper,* **44,** 181 (1986).
9. S. C. Chen and N. T. Cheng, *Int. Commu. Heat & Mass Trans.*, **18**(6), 833 (1991).
10. H. H. Chiang, K. Himasekhar, N. Santhanam, and K. K. Wang, *ASME J. Eng. Mat. & Tech.*, **115,** 37 (1993).
11. A. I. Isayev and R. K. Upadhyay, in *Injection and Compression Molding Fundamentals.* A. I. Isayev, Ed., Marcel Dekker, New York, 1987, Chapter 2.
12. R. Keunings, in *Fundamentals of Computer Modelling for Polymer Processing.* C. L. Tucker III, Ed., Hanser, New York, 1989, Chapter 9.
13. M. J. Crochet, *Rubber Chem. Tech.*, **62,** 426 (1986).
14. M. R. Kamal, E. Chu, and P. G. Lafleur, *Polym. Eng. Sci.*, **26,** 190 (1986).

15. M. R. Kamal, S. K. Goyal, and E. Chu, *AIChE J.*, **34,** 94 (1988).
16. A. I. Isayev and C. A. Hieber, *Rheol. Acta,* **19,** 168 (1980).
17. A. I. Leonov, *Rheol. Acta,* **15,** 85 (1976).
18. A. I. Leonov, *Rheol. Acta,* **15,** 411 (1976).
19. A. I. Leonov, *J. Non-Newtonian Fluid Mech.,* **25,** 1 (1987).
20. M. A. Sobhanie and A. I. Isayev, *SPE ANTEC Tech. Paper,* **35,** 286 (1989).
21. H. Mavridis, A. N. Hrymak, and J. Vlachopoulos, *J. Rheol.,* **32,** 639 (1988).
22. M. A. Sobhanie and A. I. Isayev, *Rubber Chem. Tech.,* **62,** 939 (1989).
23. A. I. Isayev and N. Famili, *J. Plast. Film & Sheet,* **2,** 269 (1986).
24. K. K. Wang, C. Cohen, D. L. Koch, C. A. Hoeber, K. Yoon, M. Gupta, and O. G. Harle, Progress Report #16 of Cornell Injection Molding Program, 1991.
25. Y. C. Chen, J. H. Wu, S. C. Chen, and J. C. Chen, *Polym. Eng. Sci.,* to appear.
26. S. C. Chen and Y. C. Chen, *J. Comp. & Struct.,* **52,** 1043 (1994).
27. Y. C. Chen, Master Thesis, Chung Yuan University, Taiwan, 1992.
28. N. T. Cheng, S. C. Chen, and K. G. Lin, submitted.

Received June 19, 1994
Accepted September 21, 1994